CENTRE DE RECERCA MATEMÀTICA

Preprint núm. 1138
January 2013

On the scaling behavior of the earthquake inter-time distribution: Influence of large shocks and time scales in the Omori law

E. Lippiello, À. Corral, M. Bottiglieri, C. Godano, L. de Arcangelis

ON THE SCALING BEHAVIOR OF THE EARTHQUAKE INTER-TIME DISTRIBUTION: INFLUENCE OF LARGE SHOCKS AND TIME SCALES IN THE OMORI LAW

EUGENIO LIPPIELLO, ÁLVARO CORRAL, MILENA BOTTIGLIERI, CATALDO GODANO AND LUCILLA DE ARCANGELIS

Abstract. We present a study of the earthquake inter-time distribution $D(\Delta t)$ for a California catalog in temporal periods of short duration T. We compare experimental results with theoretical predictions and analytical approximate solutions. For the majority of intervals, rescaling inter-times by the average rate leads to collapse of the distributions $D(\Delta t)$ on a universal curve, whose functional form is well fitted by a Gamma distribution. The remaining intervals, exhibiting a more complex $D(\Delta t)$, are all characterized by the presence of large shocks. These results can be understood in terms of the relevance of the ratio between the characteristic time c in the Omori law and T: Intervals with Gamma-like behavior are indeed characterized by a vanishing c/T. The above features are also investigated by means of numerical simulations of the ETAS model. This study shows that collapse of $D(\Delta t)$ is also observed in numerical catalogs, however the fit with a Gamma distribution is possible only assuming that c depends on the mainshock magnitude m. This result confirms that the dependence of c on m, previously observed for $m > 6$ mainshocks, extends also to small $m > 2$.

1. Introduction

The simplest description of seismicity is in terms of a point process in space, time and energy (or magnitude) and therefore a proper characterization of its temporal organization is extremely important. To this extent, Bak *et al.* [1] studied the distribution of inter-times, Δt, between successive earthquakes. Subsequently, Ref. [2] showed that, under certain conditions, inter-times in any region follow a particular probability distribution, whose shape is quite universal, i.e., independent of the geographic region and the mean seismic rate. This law can be written in mathematical terms as

$$D(\Delta t) = Rf(R\Delta t), \tag{1}$$

where $D(\Delta t)$ is the inter-time probability density and R is the mean seismic rate, defined as the number of earthquakes per unit time, and containing information about the spatial region and the minimum magnitude considered in the analysis. Note that R controls the scale of $D(\Delta t)$ but not its shape. The latter is provided by the scaling function f. Ref. [2] proposed that for stationary seismicity, i.e.,

CRM Preprint Series number 1138

when the rate R is nearly constant in time, the scaling function f can be considered universal. This scaling function, and therefore the probability density, is well approximated by a Gamma distribution

$$f(x) \propto \frac{1}{x^{1-\gamma}} e^{-x/a}, \tag{2}$$

with $x \equiv R\Delta t$. The constant of proportionality is determined by normalization, $\int_0^\infty D(\Delta t) d\Delta t = 1$. The shape parameter γ and the scale parameter a are related by $\langle x \rangle = R\langle \Delta t \rangle = R \int_0^\infty \Delta t D(\Delta t) d\Delta t = 1$, taking into account that the rate R is the inverse of the mean inter-time, $\langle \Delta t \rangle$. If the scaling function is given by Eq. (2) for all $x \geq 0$, then $\langle x \rangle = a\gamma = 1$, i.e., $\gamma = 1/a$. In the stationary case (the limit considered in Ref. [2, 3]) the best fit provides a value of γ around 0.7. The validity of Eq. (1) has been verified also for non stationary periods [4], Omori sequences [5], volcanic earthquakes [6], and even for picoseismicity [7], as well as for fracture experiments [8, 9, 10].

The existence of the scaling behavior in Eq. (1) has been subsequently addressed, by means of analytical and/or numerical investigations, in models for seismic occurrence. Molchan [11] considered a point-process model consisting in the superposition of homogeneous-Poisson mainshocks, with a rate μ, and inhomogeneous aftershocks without magnitude dependence, and found that the tail of the resulting inter-time distribution has to be exponential. Its characteristic time is determined by the inverse of the rate of the underlying Poisson process, i.e., $D(\Delta t) \propto e^{-\mu \Delta t}$ for $\Delta t \to \infty$. Rescaling by the total rate R, as in Eq. (1), gives $D(\Delta t) \propto e^{-(\mu/R)R\Delta t} = e^{-(\mu/R)x}$, which comparing with the exponential tail in Eq. (2) provides $1/a = \mu/R$. This implies that the inverse of a measures the ratio between the number of independent events (i.e., mainshocks) and the total number of events (in the window under consideration) [11]. This result is incompatible with the universal behavior of Eq. (1), unless the fraction of independent events is itself universal (at least in the stationary case). The above idea has been interestingly applied by Hainzl *et al.* [12] to an important problem in seismic hazard, i.e., the estimation of the fraction of mainshocks in a given geographic region. They evaluated the inter-time distribution in different areas of California and estimated a fitting the distribution by Eq. (2). They also generated synthetic catalogs by the ETAS model [13] and compared the experimental and numerical $D(\Delta t)$. If the two distributions coincided, they assumed that the fraction of mainshocks in the experimental catalog was given by the value of μ/R used in numerical simulations. By this approach Hainzl *et al.* obtained a map of the background rate in California.

Molchan's result has been subsequently generalized by Saichev and Sornette (SS), who analytically evaluated $D(\Delta t)$ for a superposition of a Poisson process and many Omori sequences [14, 15]. They obtained an analytical expression that generalizes Eq. (1),

$$D(\Delta t) = RG\left(R\Delta t, Rc, \mathcal{K}\right), \tag{3}$$

CRM Preprint Series number 1138

where $\mathcal{K}$ is the ratio between correlated and independent events (in the overall process, and is directly related to the branching ratio) and the time c controls the short-time behavior in the Omori law. This states that the seismic rate decays in time as $\Lambda/(c+t)^p$. SS further observed that the dependence on Rc is weak and that the functional form of $G(x, y, z)$ as a function of x is not very different from a Gamma distribution (see Section II). Conversely, $G(x, y, z)$ is strongly affected by the value of $\mathcal{K}$.

Their results, therefore, provide a possible explanation for Eqs. (1, 2) obtained in experimental catalogs. SS also derived an exact nonlinear integral equation for the distribution in the ETAS model, solved it analytically at linear order [14, 15] and developed an efficient numerical scheme to take into account nonlinear terms [16]. Their solution is in agreement with Eq. (3). A general scaling relationship, that includes also the catalog duration T, has been proposed in Ref. [17]

$$D(\Delta t) = RH\left(R\Delta t, Rc, \mathcal{K}, c/T\right) \tag{4}$$

where R is the average rate in the time interval $[0, T]$, and H is a scaling function. This scaling form has been used to enlighten the mechanisms leading to universal behavior for $D(\Delta t)$ and to explain deviations from it observed in Ref. [18]. This analysis also showed that c depends on the mainshock magnitude m as

$$c \sim 10^{\alpha' m}, \tag{5}$$

obtained for mainshocks with magnitude $m \geq 6.1$. For smaller mainshock magnitudes, the limited aftershock number does not allow a reliable estimate of c. However, an indirect indication that Eq. (5) holds also for smaller mainshock magnitude ($m > 4$) has been obtained in [17, 20]. This result, usually attributed to catalog incompleteness [19, 21], has been recently interpreted [22] in terms of correlations among earthquake magnitudes [23, 24, 25, 26, 27]. If c depends on m, the value of c/T in Eq. (4) has to be understood in an averaged way, see Sec. III.

In this paper, differently from previous studies that consider long temporal intervals but restricted geographical regions, we study $D(\Delta t)$ in short temporal intervals. More precisely we subdivide the relocated Southern California Catalog [28] (years 1981-2011) in 50 temporal intervals all containing the same number of events. We observe that for 43 intervals the scaling behavior Eq. (1) holds with the scaling function in good agreement with a Gamma distribution with $\gamma \simeq 0.57$. Since R presents huge fluctuations from interval to interval, whereas the Poisson rate μ is expected to be roughly constant in time, the validity of the scaling behavior Eq. (1) indicates that the asymptotic decay of $D(\Delta t)$ is not controlled by μ. For these intervals it is reasonable to assume $c/T \simeq 0$ and the arguments by SS (Eq. (3)) can be used to explain the observed universal behavior. However, we stress that the scaling function is better fitted by a Gamma distribution than by the function $G(x, y, z)$ obtained by SS. Non universal behavior is conversely observed for the remaining 7 intervals, all characterized by the presence of large

shocks. In this case, c is comparable to, or even larger than T and deviations from universality can be attributed to the fact that c/T does not tend to zero. Nevertheless, it turns out to be that Eq. (4) is no longer valid but other time scales, related to the temporal position of the mainshock in the interval, must be included in the scaling behaviour.

The same problem is investigated by numerical simulations of the ETAS model. More precisely, together with the standard ETAS model, we also perform numerical simulations for the case where c scales with the mainshock magnitude according to Eq. (5). Numerical simulations confirm the separation of intervals in two classes: those containing large shocks with evident violations of Eq. (1) and the large majority of intervals where Eq. (1) is satisfied. Restricting the analysis to intervals fulfilling scaling, we observe that in simulations for constant c, the scaling function $f(x)$ is very well fitted by the analytical $G(x, y, z)$ obtained by SS. Conversely, in simulations where c depends on m, $f(x)$ is better fitted by a Gamma distribution in accordance with results from the experimental catalog. This result supports the dependence of c on the mainshock magnitude also for mainshocks with $m > 2$.

The paper is organized as follows. In Section II we review the main results by Molchan and Saichev & Sornette. In Sec. III we apply a Kolmogorov-Smirnov test to identify the inter-time distributions that, after rescaling, collapse onto each other and can therefore be fitted by a common distribution with only different scale parameters. In Sec. IIIA we present experimental results for the 43 intervals exhibiting scaling behavior, in Sec. IIIB we present a simple explanation for deviations from universality in intervals including large mainshocks, and in Sec. IIIC we confirm this explanation. In Sec. IV we discuss results from numerical simulations of the ETAS model and final Conclusions are drawn in the last Section.

2. Analytical results

As discussed previously, Molchan derived some general analytical properties of the inter-time distribution for a simple point process in time, without space or magnitude dependence. The model assumed mainshock occurrence to be a homogeneous Poisson process in time, whereas an inhomogeneous point process generated clusters of events associated to each independent mainshock. Molchan then investigated the asymptotic behavior of the inter-time distribution for the temporal sequence of events resulting from the superposition of the two processes. He proved that, quite independently of the temporal dependence of the rate in the inhomogeneous process, the inter-time distribution exhibits at long times an exponential decay controlled by the value of the homogeneous Poisson rate. Conversely, the distribution behavior at short times is dominated by the rate of clustered events after the mainshocks.

CRM Preprint Series number 1138

Saichev and Sornette also questioned the validity of universal scaling for the inter-time distribution within the context of branching models. Their approach supposed that independent events (mainshocks) occur at constant rate μ and each event can trigger a number $n < 1$ events in a subcritical regime. These are the first generation aftershocks, which may trigger n higher generation events each, and so on. The rate of triggered events is described by the Omori law (assumed to be self-averaging), whereas the productivity law is neglected, i.e., they assume that each earthquake triggers, on average, the same number of events independently of its magnitude. Under these approximations, SS obtained that the inter-time distribution depends on the rate R, the characteristic time c and the fraction of correlated events $\mathcal{K}$ according to Eq. (3) with the function $G(x, \epsilon, \mathcal{K})$ given by

$$G(x,\epsilon,\mathcal{K}) = \left(\frac{\mathcal{K}}{(\mathcal{K}+1)\epsilon} \left. \frac{\partial^2 A(w)}{\partial w^2} \right|_{w=\frac{x}{\epsilon}} + \frac{1}{(\mathcal{K}+1)^2} \left(1 + \mathcal{K} \left. \frac{\partial A(w)}{\partial w} \right|_{w=\frac{x}{\epsilon}} \right)^2 \right) \exp\left(\frac{1}{\mathcal{K}+1} \left(-x - \mathcal{K}\epsilon A\left(\frac{x}{\epsilon}\right) \right) \right) \tag{6}$$

with $\epsilon = Rc$, $A(w) = \left((1+w)^{2-p} - 1\right)/(2-p)$, and $x = R\Delta t$. The dependence of G on p is obviated, as it is assumed that p is close to 1.

3. Classification of inter-time distribution evaluated in different temporal windows

We study Southern California's seismicity using the Waveform Relocated Earthquake Catalog of this region, covering a rectangular box of coordinates (122°W, 30°N), (113°W, 37.5°N) from January 1st, 1981 to June 30th, 2011 (downloaded from the Southern California Earthquake Data Center [28]). This catalog contains 111981 events with $m \geq 2$.

We divide the catalog into $N_{int} = 50$ intervals, each containing 2239 events, and we disregard a remainder of 31 events. In each of these intervals we compute the inter-time probability distribution, removing inter-times smaller than 10 seconds since their values are severely affected by uncertainty, also due to short term catalog incompleteness [19]. Six inter-times associated to holes in the catalog in the years 1981 and 1983 (the longest lasting 34 days, the shortest about 3 days) are also removed from the distributions.

In order to compare the shape of the distributions for different intervals, we calculate the mean inter-time for each distribution, $\langle \Delta t \rangle$, and rescale inter-times in each interval by this mean value, i.e., $x \equiv \Delta t / \langle \Delta t \rangle$. We consider all pairs of rescaled distributions, and for each couple we limit the analysis to the range of x common to both functions, namely, we neglect the smallest values of x

CRM Preprint Series number 1138

contributing to only one of the two distributions. Then, we compute again the mean of each distribution (which, at this step, will be close to one) and rescale it again by its mean.

Next, for each couple of distributions, we perform a 2-sample Kolmogorov-Smirnov test [29], which computes a "distance" between two experimental distributions, using their cumulative representation. A $P-$value computed analytically [29], determines if the distance is large (P small) and the distributions are not compatible, or else if the distance is small (P large) and the distributions are compatible with the same functional form, independently of their scale. Notice that this approach will provide an estimation of the agreement of two distributions only in the common range of x; namely, we are not testing if each pair of distributions are the same, but if for a certain range of x they have a similar shape, independently of scale parameters [30]. Although the rescaling by the empirical value of Δt introduces a small bias in the procedure, this is not relevant for our relative comparison. We also stress that no fit is involved in the process, at this stage.

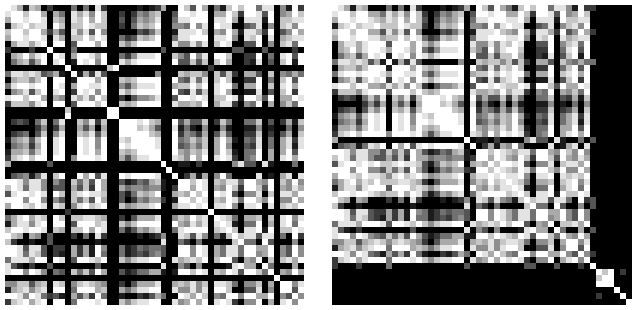

FIGURE 1. (color online) (a) Matrix of earthquake inter-time distribution similarity between the 50 time intervals in which the California catalog is divided. The intervals run from top to bottom and from left to right. White corresponds to $P-$values larger than 10^{-1}, black to $P \leq 10^{-10}$, and grey indicates intermediate values in logarithmic scale. (b) The same, but moving the intervals 8, 11, 18, 19, 28, 35, and 46 to the bottom right corner, in order to separate them from the connected class. The compatibility between 11, 18, and 19 is also apparent.

The $P-$values for each couple of distributions allow to define a matrix of similarity, or connectivity, between the intervals, see Fig. 1(a). We can then separate the intervals into two broad classes: The first one is a connected class, in the sense that all intervals in this class are linked through $P-$values larger than 0.01.

CRM Preprint Series number 1138

More precisely, if we define a network of intervals characterized by similar distributions, i.e. connected only by $P-$values larger than 0.01, we could find a path from each interval to any other interval of the connected class. The other class obviously contains those intervals disconnected from the previous class; indeed, the strongest connection between the two classes (i.e., the largest $P-$value) is about $5 \cdot 10^{-6}$. These "non-connected intervals" have temporal labels 8, 11, 18, 19, 28, 35, 46. Figure 1(b) shows clearly this separation.

As we are performing multiple testing (the number of couples is $50 \cdot 49/2 = 1225$), the effective significance level for each test has to be reduced, according to the Bonferroni correction, by a factor $1/1225$ in order to keep the original global significance level [31, 32]. For instance, if the latter is selected at 0.05, this yields for the former a value $4 \cdot 10^{-5}$. This implies that the six incompatible intervals (separated from the connected class by $P-$values below $5 \cdot 10^{-6}$) still remain incompatible (as they are below the effective significance level), but the connections in the connected class are stronger than what the 0.01 minimum value suggests (as the rejection limit has dropped to $4 \cdot 10^{-5}$).

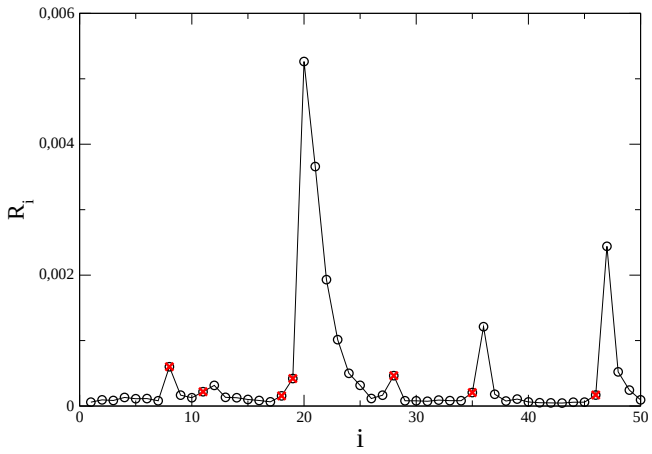

FIGURE 2. (color online) Mean seismic rates in California for each time interval i, measured in earthquakes per second. Red marks denote non-Gamma intervals. As an indication, the Landers earthquake (1992) occurs in the 19th interval.

In the following we define as Gamma intervals those intervals for which the Kolmogorov-Smirnov test gives results compatible with the connected class. The reason is that the resulting distributions are well fitted by a Gamma distribution. Conversely, we define as non-Gamma intervals the other temporal periods. In Fig. 2 we plot the rate R_i in different intervals and indicate with red marks the non-Gamma intervals. This figure shows that the seismic rate does not allow to discriminate between Gamma and non-Gamma intervals.

CRM Preprint Series number 1138

3.1. **Gamma Intervals.**

In Fig. 3 we plot the rescaled $D(\Delta t)$ for all Gamma intervals including all Δt larger than 1 sec. We can see that the scaling behavior Eq. (1) is fulfilled with small deviations only at small values of $R\Delta t$. Except for the small Δt region, the fit with the Gamma distribution very well reproduces the experimental distributions. In particular we find that the best fit is provided by $\gamma = 0.57 \pm 0.02$ in Eq. (2).

In the following we consider among all intervals, four sets with different values of R_i. The choice of other intervals leads to the same conclusions. This analysis is performed in order to verify the predictions by Molchan and SS. According to Molchan's argument, we should expect an asymptotic behavior $D(\Delta t) \sim \exp(-\mu \Delta t)$ and, since μ is about constant in time, this would imply the collapse of the distribution tails for different intervals (at least in the horizontal axis). In Fig. 4 we plot $D(\Delta t)$ versus Δt for the four intervals without rescaling and show that the distribution tails do not collapse. In the inset we explicitly show that the asymptotic decay is consistent with a pure exponential but with a slope different for each interval. Excellent collapse is conversely observed if we rescale time by the rate (Fig. 5). In this case Eq. (1) is fulfilled with the scaling function well fitted by a Gamma distribution (except at very small Δt). This is confirmed in the inset of Fig. 5 where we plot $\Delta t D(\Delta t)$, as suggested in Ref. [18, 17], to enlighten deviations from pure Gamma-like behavior. Consistently with previous findings [18, 17, 30], deviations from Gamma-like behavior are observed only at $R\Delta t < 10^{-3}$.

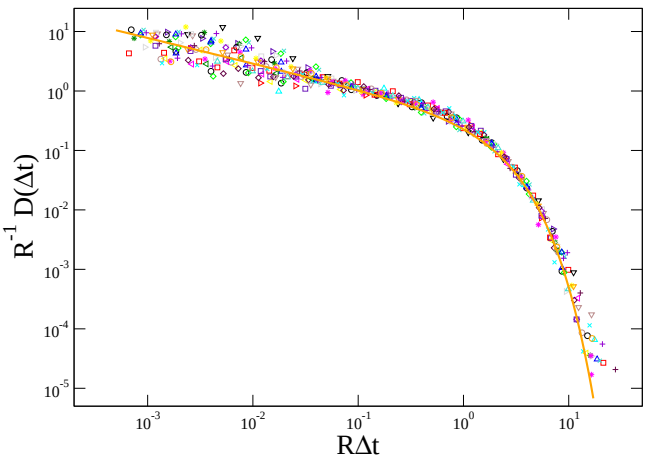

FIGURE 3. (color online) Rescaled earthquake inter-time probability densities for the 43 Gamma intervals in California. The orange continuous line is the fit with a gamma distribution with $\gamma = 1/a = 0.57$. Inter-times below 10 s are not plotted.

Next we test the prediction by SS. We implement a wide range of values for the parameters c, $\mathcal{K}$, and μ (which changes the resulting R) and select their values in Eq. (6) looking for the best agreement between experimental and analytical curves. We first verify that, even taking into account fluctuations of $R = R_i$ at fixed c, the dependence on Rc is very weak and curves for different R_i collapse onto each other. Therefore, the argument by SS may explain the collapse of Figs. 3-5. However, we wish to stress that the comparison between the fit by a simple Gamma distribution with the fit by Eq. (6), indicates that the SS fit gives a better agreement at small x, whereas the fit with a pure Gamma distribution better performs at large x. We attribute the discrepancy between Eq. (6) and experimental results to the existence of c depending on the mainshock magnitude, which is not taken into account by SS. This interpretation will be confirmed by numerical simulations of the ETAS model (Sec. IV).

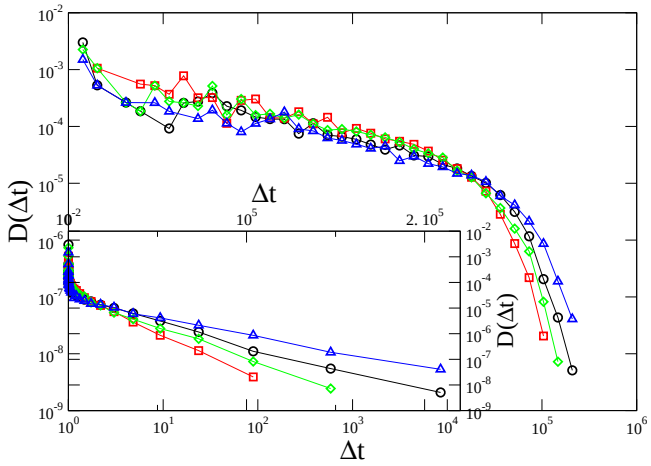

FIGURE 4. (color online) Earthquake inter-time probability densities of 4 representative intervals (temporal labels 17, 26, 32, and 43) of the Gamma class, for California. Time units are seconds. The distribution tails make apparent that the exponential decay is different in each case. Inset: the same curves on logarithmic-linear scale.

3.2. **Non-Gamma intervals.**

Each non-Gamma interval (indicated in Fig. 2 by red marks) includes large mainshocks but, in general, these intervals do not correspond to periods of maximum rate. Largest shocks present in each interval are listed in Table 1. As discussed later, the presence of large shocks makes the argument c/T relevant in Eq. (4) and this is one of the causes for deviations from the scaling Eq. (1). But in addition, $D(\Delta t)$ is also controlled by the temporal position of the mainshock in the interval. A simple argument can be developed to understand the functional form of $D(\Delta t)$

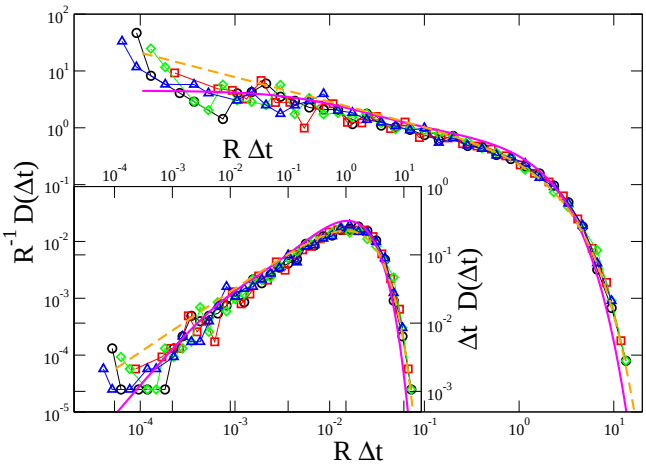

FIGURE 5. (color online) The same distributions as in the previous plot, rescaled by the mean rates R. The SS fit (magenta continuous line) and the Gamma fit (dashed orange line) are also shown, with parameters $\mathcal{K} = 2.3$, $p = 1.05$, $c = 100$ s, and $\mu = 10^{-4}$ s^{-1} (SS) and $\gamma = 1/a = 0.57$ (Gamma). Inset: the same distributions, multiplying the ordinate by Δt.

in these intervals. For an inhomogeneous Poisson process for which the rate is large enough compared to its relative rate of change, the inter-time distribution can be obtained from the distribution of rates $\rho(r)$ via the relation [33]

$$D_i(\Delta t) = \frac{1}{R_i} \int dr \rho_i(r) r^2 \exp(-r\Delta t). \tag{7}$$

We indicate with t_i the starting time of the i-th interval and T_i its duration. Assuming that a mainshock occurs at a time $t_0 \in [t_i, t_i + T_i]$ we define $\beta = (t_0 - t_i)/T_i$ as the fraction of time in the i-th interval before the mainshock. As a consequence $1-\beta$ is the fraction of time after mainshock occurrence. In intervals including large mainshocks the rate is very high and, since the number of events in each interval is fixed, this implies small values of $t_i + T_i - t_0$. On the other hand, according to Eq. (5) we expect large c values, therefore it is reasonable to assume $c \gg (t_i + T_i - t_0)$. Under this assumption, we indicate with $\lambda_c = \Lambda c^{-p}$ the rate of events after the mainshock and $\rho(r)$ can be written as

$$\rho(r) = \beta \rho_G(r) + (1-\beta)\delta(r - \lambda_c), \tag{8}$$

where ρ_G is the rate distribution before mainshock occurrence. Introducing the above expression in Eq. (7) we obtain

$$D(\Delta t) = \frac{\lambda_G^2 \beta f(\lambda_G \Delta t) + (1-\beta)\lambda_c^2 e^{-\lambda_c \Delta t}}{\beta \lambda_G + (1-\beta)\lambda_c} \tag{9}$$

CRM Preprint Series number 1138

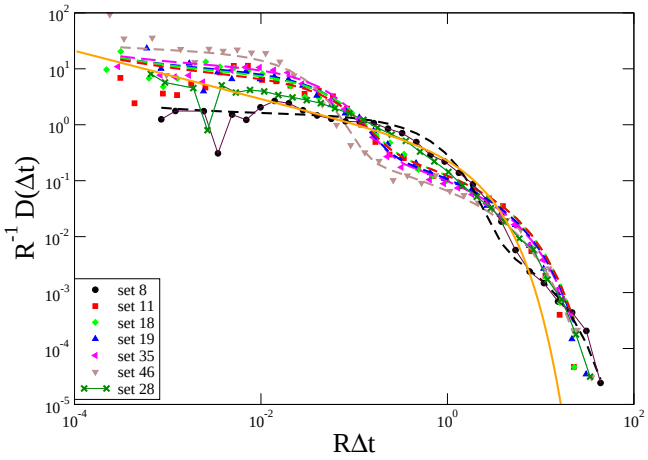

FIGURE 6. (color online) Rescaled earthquake inter-time probability densities for 7 intervals in California not belonging to the Gamma class, together with their fits (dashed lines). The fit with the Gamma distribution is also shown (continuous orange line).

where λ_G is the average rate in the sub-interval before mainshock occurrence and $f(x)$ the scaling function in the interval $[t_i, t_0)$. Different scaling behaviors are therefore expected for different values of β, i.e., different positions of the mainshock within the interval. Next, we assume that $f(x)$ is given by a Gamma distribution in agreement with the fit in Figs. 3-5. Moreover, since $\lambda_c \gg \lambda_G$, λ_G can be obtained from the tail of the distribution, whereas λ_c can be inferred from the rate soon after mainshock occurrence. Finally, β can be directly obtained from the experimental catalog and we can apply Eq. (9) to fit the experimental distribution. Results plotted as dashed lines in Fig. 6 support the validity of the above arguments. Only for interval 28 (continuous line) the inter-time distribution is not consistent with Eq. (9). This can be justified by observing that interval 28 immediately follows the Northridge earthquake, occurring just at the end of interval 27. In this particular case, $\beta = 0$ but the ratio c/T is smaller than one and therefore the distribution cannot be fitted by a pure exponential.

It is interesting to discuss the two limiting cases $\beta = 1$ and $\beta = 0$. In particular we evaluate the $D(\Delta t)$ separately in two intervals containing both $N_e = 2000$ events, chosen just before, $D_{before}(\Delta t)$ ($\beta = 1$), and just after ($\beta = 0$), $D_{after}(\Delta t)$, the large Hector Mine ($m = 7.1$) earthquake. In Fig. 7 we compare these two distributions with the distribution evaluated for the merged subsets with $N_e = 4000$ events. The distributions for events before and after the Hector Mine earthquake have very different temporal extensions, with the maximum value of Δt before the Hector Mine earthquake greater than the maximum Δt after the mainshock. The whole distribution is dominated by $D_{after}(\Delta t)$ at small Δt and by $D_{before}(\Delta t)$ at large inter-times. It is quite evident that the functional form of $D(\Delta t)$ for

CRM Preprint Series number 1138

the merged interval is very different from both distributions evaluated for the separate subsets.

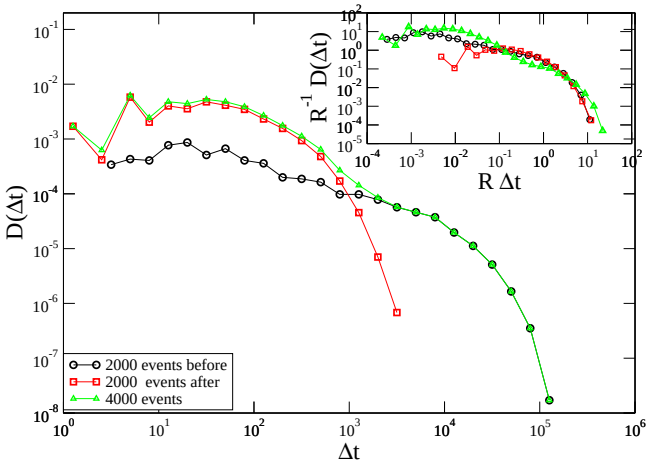

FIGURE 7. (color online) Inter-time probability densities around the Hector Mine earthquake (1999). Red squares corresponds to 2000 events after the mainshock, black circles to 2000 events before the main, and the green triangles to 4000 events including the main in the middle of the list of events in the interval. The latter distribution is multiplied by a factor 2 to allow a better comparison. Time units are seconds. The inset shows the same curves under rescaling by R.

However, rescaling inter-times by the average rate in each interval (inset of Fig. 7), a collapse consistent with Eq. (1) is obtained for D_{before} and D_{after}. The function $f(x)$ takes values over different rescaled temporal domains for events before and after the main-shock (black circles and red squares), but data follow the same functional form $f(x)$. Conversely, the functional form for the merged subsets is clearly different (green triangles). Fig. 7 confirms our interpretation for the mechanisms leading to deviations from simple scaling Eq. (1). In the temporal interval before the mainshock $f(x)$ is not affected by c/T and is consistent with Eq. (3). After the mainshock, conversely, the scaling is controlled by c/T and, since $c/T \sim 1$, being the rate almost constant, $f(x)$ is well approximated by an exponential (as can be derived from Eq. (7)). Merging the two intervals, the resulting distribution does not collapse on the previous curves. Very similar results are obtained for other mainshocks.

3.3. **Discrimination between Gamma and Non-Gamma intervals.**

According to the above study, the contribution from c/T should discriminate between Gamma intervals ($c/T \ll 1$) from non-Gamma intervals when the term

c/T becomes non-vanishing. We first verify this result considering different partioning of the catalog, namely different N_{int}. Smaller values of N_{int} lead to larger values of T but do not affect c. We find that deviations from Eq. (1) become less relevant by decreasing N_{int} and in particular for $N_{int} = 5$ all 5 curves collapse onto each other; nevertheless, the gamma fit leads to a different value of the $\gamma-$parameter, explained by the term Rc in Eq. (3).

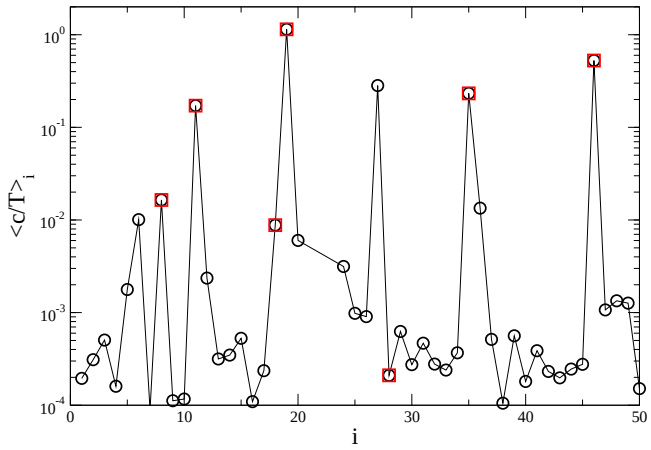

FIGURE 8. (color online) The average value $\langle c/T\rangle_i$ defined in Eq. (11) for each time interval i. Red marks denote non-Gamma intervals

To further investigate the role of the ratio c/T, we notice that a direct measurement of c/T in each interval is not possible since it is very difficult to evaluate c for small or intermediate mainshock magnitudes ($M \lesssim 6$). In this case, indeed, the number of aftershocks is not sufficiently large to measure c in the Omori decay. In the following we assume that the experimental relationship between c and the mainshock magnitude m (5) experimentally observed only for large m, holds for any mainshock magnitude. More precisely, we assume the result obtained in Ref. [19],

$$c = 10^{m-6} \tag{10}$$

where c is measured in days. Numerical simulations of the ETAS model support the validity of Eq. (10) for all mainshock magnitudes. The following step is the use of a declustering method to discriminate between independent mainshocks and aftershocks. We use the declustering algorithm of Ref. [34] where an event is identified as a mainshock if it is sufficiently isolated in time and space from larger shocks. In particular we assume that an event is a mainshock only if no larger event has occurred 30 days before or 3 days after in a radius of 200 kms.

CRM Preprint Series number 1138

Once mainshocks are identified, in each interval i, we evaluate the quantity

$$\langle c/T\rangle_i = \frac{1}{N_{main}(i)} \sum_{k=1}^{N_{main}(i)} \frac{10^{m_k-6}}{t_{i+1}-t_{0k}} \tag{11}$$

where $N_{main}(i)$ are the number of mainshocks in the i-th interval, t_{i+1} the final time of the interval and m_k and t_{0k}, the magnitude and occurrence time, respectively, of the k-th mainshock in the interval i. Results of Fig. 8 show that in the large majority of intervals $\langle c/T\rangle_i \ll 1$. In all these intervals Eq. (1) is fullfilled and $f(x)$ is well fitted by a Gamma function. Conversely, intervals where $\langle c/T\rangle_i > 0.01$ correspond to non-Gamma intervals. The only exception is for interval 27 where, as explained before, the mainshock has occurred at the end of the interval. Therefore, non-Gamma behavior of $D(\Delta t)$ is obtained in the interval 28 but a finite value of $\langle c/T\rangle_i$ is observed in the interval 27.

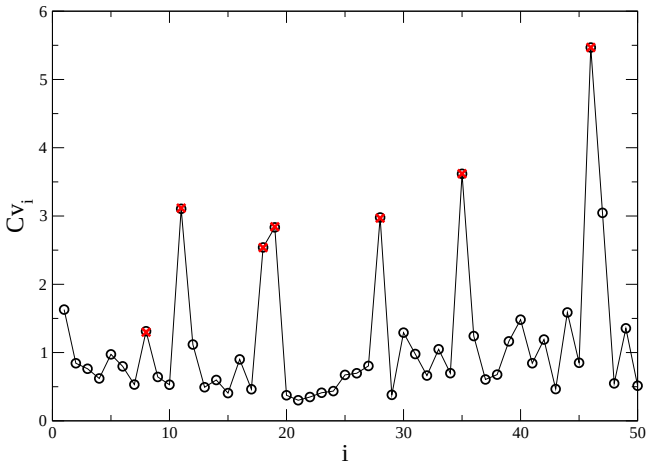

FIGURE 9. (color online) The variability coefficient of the seismic rate for each time interval, calculated partitioning each interval in $M = 20$ subintervals. Red marks identify intervals with anomalous (i.e., non-Gamma) inter-time distributions.

In the following we develop another criterion allowing the discrimination between Gamma and non-Gamma intervals. Non-Gamma behaviour is indeed expected for intervals where the rate abruptly changes because of large mainshocks. In order to characterize the variability of the rate, we introduce the variability coefficient, related to the second moment of the rate distribution

$$Cv(i) = \frac{\sqrt{\langle r^2(i)\rangle - \langle r(i)\rangle^2}}{\langle r(i)\rangle}. \tag{12}$$

CRM Preprint Series number 1138

To evaluate $Cv(i)$ we divide the i-th interval in $M = 20$ sub-intervals of equal duration dt and define the moments of the rate distribution as

$$\langle r^2(i)\rangle = \frac{1}{M}\sum_{j=1}^{M} r_j^2 \tag{13}$$

and

$$\langle r(i)\rangle = \frac{1}{M}\sum_{j=1}^{M} r_j \equiv R_i \tag{14}$$

where $r_j = n_j/dt$ and n_j is the number of earthquakes in the j-th subinterval. $Cv(i)$ (Fig. 9) assumes small values in the majority of intervals and presents some maxima with values larger than 2. A value of $Cv(i)$ close to $1/\sqrt{R_i T_i}$ ($\simeq 0.02$ in our case) is the signature of a Poisson process, with $\mu = R_i$. Conversely, larger values of $Cv(i)$ indicate that the rate assumes larger variability than in a Poisson process. The maxima correspond to periods with large rate variability and indeed very well identify non-Gamma intervals, indicated by red marks in Fig. 2.

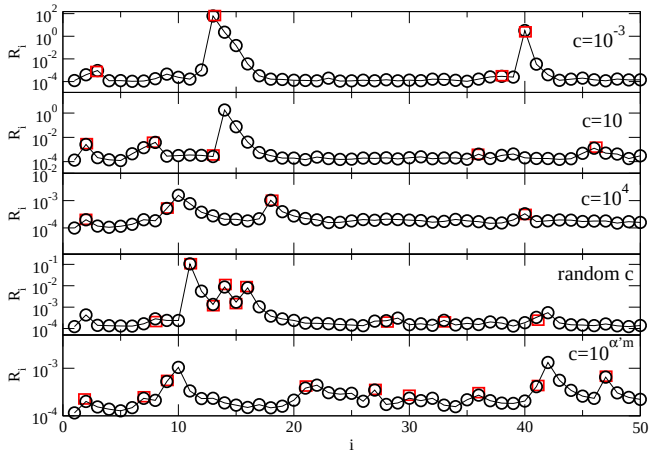

FIGURE 10. (color online) Mean rate of events in the simulations of the ETAS model for different choices of c, as a function of the time interval number. From top to bottom, we take $c = 10^{-3}, 10, 10^4$ s, c fluctuating for each sequence in the interval $[10^{-3}, 10^2]$ s and c dependent on the mainshock magnitude according to Eq. (5). Red squares indicate intervals with non-Gamma $D(\Delta t)$.

CRM Preprint Series number 1138

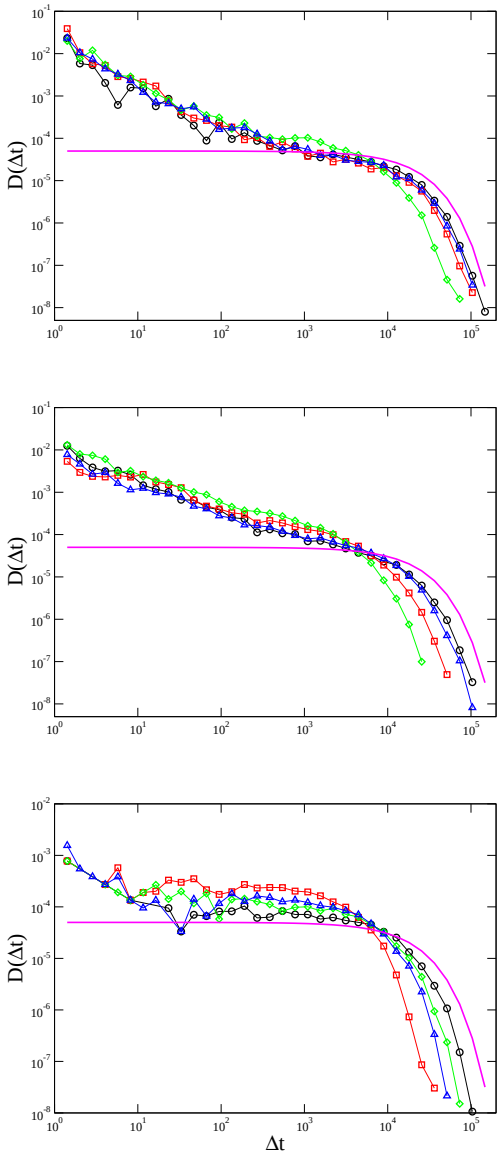

FIGURE 11. (color online) Inter-time probability densities of events in the simulations of the ETAS model, for 4 representative non-anomalous intervals. Numerical simulations are performed with parameters $\mathcal{K} = 2.3$, $p = 1.05$, $\mu = 5.3 \cdot 10^{-5}$ s^{-1}, and three different values of c equal to 10^{-3} s, 10 s and 10^4 s, from top to bottom. The exponential distribution corresponding to the underlying Poisson process with $\mu = 5.3 \cdot 10^{-5}$ s^{-1} is also shown as a continuous line.

CRM Preprint Series number 1138

4. Numerical simulations of the ETAS model

In the following we present results of numerical simulations of the ETAS model. We follow the numerical procedure proposed in [35]. We start by generating N_m independent mainshocks that occur randomly in time within the interval $[0, T_{tot}]$. The Poisson rate is therefore given by $\mu = N_m/T_{tot}$. In particular, we choose $T_{tot} = 18$ years and $N_m = 30000$. Results do not depend on these parameter values. Mainshock magnitudes m are assigned according to the Gutenberg-Richter distribution 10^{-bm} with $m \geq 2$. Each mainshock of magnitude m triggers a number of first generation aftershocks n_{after} given by the productivity law [36], $n_{after} = K10^{\alpha m}$. Aftershock magnitudes and occurrence times are assigned according to the Gutenberg-Richter law and the Omori law. Each first generation aftershock is then considered as a potential mainshock of second generation aftershocks. These aftershocks are generated according to the same laws modeling the occurrence in magnitude and time of first generation aftershocks. The procedure is then iterated until no further aftershock is triggered. A sorting procedure is finally applied to the simulated catalog. We set $\alpha = b = 1$ and $p = 1.05$, whereas K in the productivity law is fixed imposing that the total number of events in the synthetic catalog equals the number of $m \geq 2$ earthquakes in the Southern California experimental catalog.

We have considered different choices for c. In the first set of simulations we fix c to a constant value and results are presented for three different values $c = 10^{-3}, 10, 10^4$ s. In the second set we implement a c randomly fluctuating from sequence to sequence, $c \in [10^{-3}, 10^2]$ s. In the third set we take c dependent on the mainshock magnitude according to Eq. (5). In particular the best agreement with experimental data is obtained for $c = 0.4 \times 10^{0.8m}$ s. In all cases we always find that, after rescaling by the rate, the inter-time distributions exhibit a very good data collapse in most of the temporal intervals. Only intervals characterized by the presence of large shocks exhibit a different functional form always consistent with Eq. (9). In Fig. 10 we show the rate in each interval for the different choices of c. Red squares indicate intervals with non-Gamma $D(\Delta t)$. In the following we explore the behavior of the inter-time distribution in Gamma intervals.

4.1. **Gamma intervals.**

In order to compare numerical results with experimental findings plotted in Figs. 4 and 5, we first consider the inter-time distributions without rescaling by the rate (Fig. 11). We start by discussing the case with fixed c. For each value of c we consider four intervals (in the Gamma class) with different values of R_i. In the numerical catalog the rate μ of Poisson events is exactly known and therefore we can explicitly verify Molchan's prediction concerning the asymptotic decay of $D(\Delta t)$. As already observed for the experimental catalog, the tail of the distribution is different from the exponential decay $\exp(-\mu\Delta t)$ and, furthermore, it depends on the particular interval.

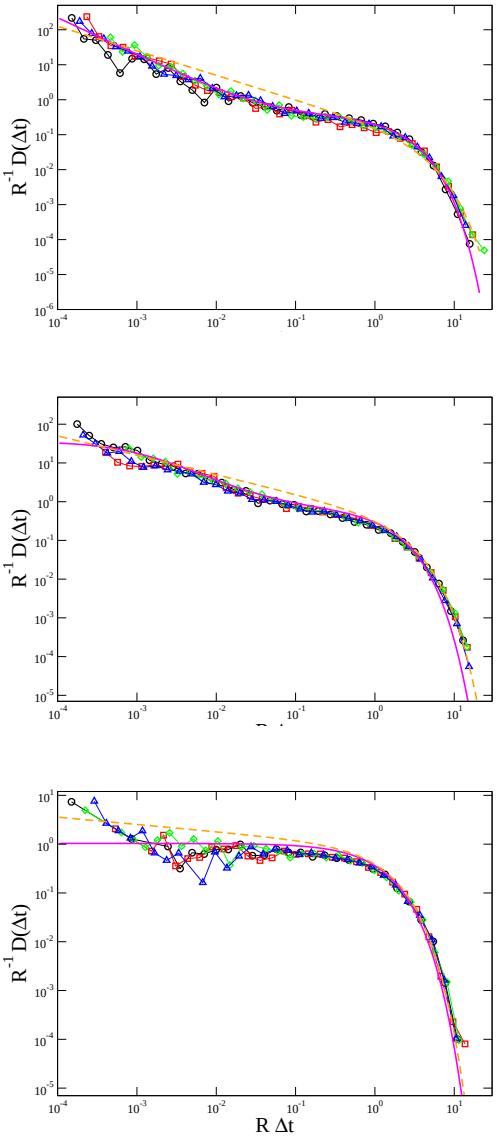

FIGURE 12. (color online) Same curves as in the previous plot, rescaling by the mean seismic rate. Fits with the SS formula (continuos magenta line) and with a Gamma distribution (dashed orange line) are also shown. The parameters in Eq. (6) are $\mathcal{K} = 2.3$, $p = 1.05$, $\mu = 5.3 \cdot 10^{-5}$ s^{-1} and c equal to 10^{-3} s, 10 s and 10^4 s from top to bottom. Best fit with a Gamma distribution are given by $\gamma = 1/a = 0.3, 0.5, 0.85$ from top to bottom.

In Fig. 12, we present the same data rescaled by the rate R_i. In this case we obtain a very good collapse for all values of c. For numerical data all the parameters in Eq. (6) are exactly known and we can compare numerical data with

CRM Preprint Series number 1138

the analytical expression Eq. (6). Results plotted in Fig. 12 show an excellent agreement for all values of c. According to Eq. (6), exact collapse for intervals with different R_i is not expected because of the combined dependence on $R_i c$. Nevertheless, as already observed by SS, for typical parameters the dependence of Eq. (6) on $R_i c$ is so weak that deviations from the collapse are negligible. We have explicitly verified that the quality of the collapse is substantially unaffected if other values of R_i are used in Eq. (6). For each choice of c the analytical expression Eq. (6) very well reproduces the numerical distribution. The above analysis suggests [14] that scaling Eq. (1) (Fig. 12) is not rigorously exact but is an excellent approximation. In Fig. 12 we have also superimposed the Gamma distribution obtained as best fit of experimental curves in Figs. 3, 5. The best agreement with the Gamma fit is obtained for the intermediate value of c. Nevertheless, also in this case the quality of the fit with a Gamma distribution is worse than for experimental curves (Fig. 5). Since the functional form of the scaling function $f(x)$ is strongly affected by c, we attribute this discrepancy to the fact that in the real catalog c is not constant.

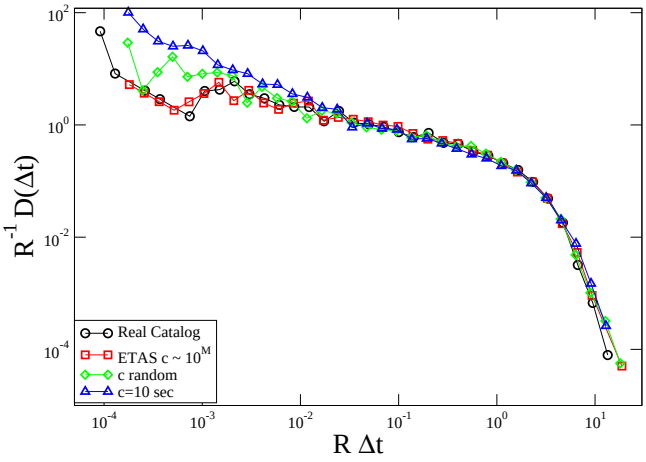

FIGURE 13. (color online) Rescaled inter-time probability densities of events in the California seismic catalog and in simulations of the ETAS model, for a representative Gamma interval.

In Fig. 13 we present results for simulations with c given by Eq. (5). Also in this case the overall behavior of Figs. 10, 11 is recovered, namely the collapse according to the scaling Eq. (1) is observed for the majority of intervals. Concerning the functional form of $f(x)$, in Fig. 13 we compare the experimental $D(\Delta t)$ with the numerical one evaluated in three different ETAS catalogs: with $c = 10$ s, random c in the interval $[10^{-3} : 10^{2}]s$ and c given by Eq. (5). For each catalog we choose the inter-time distribution evaluated in one interval, considered representative of all other Gamma intervals. The inter-time distribution for $c = 10$ s well

reproduces the tail of the experimental distribution ($R\Delta t \gtrsim 0.1$) but it is above the experimental distribution at small Δt. Larger values of a constant c lead to a flatter $D(\Delta t)$ at small Δt but introduces deviations from the experimental $D(\Delta t)$ at intermediate and large Δt ($R\Delta t \gtrsim 1$). Implementing a random c, differences at small Δt are significantly reduced. Interestingly, simulations with c depending on the mainshock magnitude lead to an inter-time distribution in very good agreement with the experimental one. Therefore deviations of Eq. (6) from the fit with a Gamma distribution, as well as deviations from the experimental $f(x)$, can be attributed to the approximation of a constant c in the SS analytical derivation.

5. Conclusions

We have investigated the existence of universal scaling behavior for the earthquake inter-time distribution by studying its behavior in short temporal intervals. We have partitioned the California catalog in temporal intervals with the same number of events and we have shown, by a Kolmogorov-Smirnov test, that the inter-time distribution scaling behavior, previously observed for different geographical areas in long temporal intervals, is also observed for the majority of these intervals. In order to understand the origin of anomalous behavior measured in some intervals, we have introduced the rate variability coefficient as a criterion to discriminate between intervals where $D(\Delta t)$ obeys the scaling Eq. (1), and the other intervals. We have then proposed an interpretation for both the mechanisms leading to deviations from Eq. (1) in some intervals and the collapse in other intervals in terms of the level of rate variability within each interval. Comparing with analytical results by SS and numerical simulations of the ETAS model, we conclude that the collapse by Eq. (1), even if not rigorous (in the context of the ETAS model), represents an excellent approximation. Anomalous behavior is conversely observed if a large mainshock is present within the temporal interval. Numerical simulations of the ETAS model also indicate that the Gamma-like behavior of the scaling function, obtained in the experimental catalog, can be attributed to a c dependent on the mainshock magnitude m. The agreement between experimental results and numerical simulations with c depending on m, confirms that the dependence of c on the mainshock magnitude, obtained for $m > 6$ mainshocks, occurs also for small ($m > 2$) mainshocks. The above results further confirm that the time constant c strongly affects the functional form of the inter-time distribution. Furthermore, we have shown that the implementation of a non-constant c in forecasting models contribute to better reproduce the temporal organization of seismicity.

Our use of the Kolmogorov-Smirnov test arised from the collaboration of one of us with R. Ferrer-i-Cancho. We learned about the Bonferroni correction through P. Puig. E.L., L.d.A. and C.G acknowledge the financial support of MIUR–FIRB

Interval	Earthquake	Magnitude	Date
8	$NorthPalmSprings$	5.72	1986/07/08
11	$SuperstitionHill$	6.6	1987/11/24
18	$JoshuaTree$	6.1	1992/04/23
19	$Landers$	7.3	1992/06/28
28	$Northridge$	6.7	1994/01/17
35	$HectorMine$	7.1	1999/10/16
46	$BajaCalifornia$	7.2	2010/04/04

TABLE 1. Largest shocks present in non-Gamma intervals.

RBFR081IUK (2008) and MIUR–PRIN 20098ZPTW7 (2009), A.C. acknowledges Spanish projects FIS2009-09508 and 2009-SGR-164.

REFERENCES

[1] P. Bak, K. Christensen, L. Danon, and T. Scanlon, Phys. Rev. Lett. **88**, 178501, (2002).
[2] A. Corral, Phys. Rev. Lett. **92**, 108501, (2004).
[3] A. Corral, Phys. Rev. E **71**, 017101, (2005).
[4] A. Corral, Tectonophys. **424**, 177, (2006).
[5] R. Shcherbakov, G. Yacovlev, D. L. Turcotte and J. B. Rundle Phys. Rev. Lett. **95**, 218501, (2005).
[6] M. Bottiglieri, C. Godano, and L. D'Auria, J. Geophys. Res. **114**, B10309, (2009).
[7] J. Davidsen and G. Kwiatek, preprint (2012).
[8] J. Davidsen, S. Stanchits, and G. Dresen, Phys. Rev. Lett. **98**, 125502, (2007).
[9] J. Åström, *et al.* Phys. Lett. A **356**, 262–266, (2006).
[10] G. Niccolini, G. Durin, A. Carpinteri, G. Lacidogna, and A. Manuello, J. Stat. Mech. **P01023**, 1–11, (2009).
[11] G. Molchan, Pure Appl. Geophys. **162**, 1135–1150, (2005).
[12] S. Hainzl, F. Scherbaum, and C. Beauval, Bull. Seismol. Soc. Am. **96**, 313–320 (2006).
[13] , Y. Ogata, *Ann. Inst. Stat. Math* **50**, 379, (1998); Y. Ogata and J. Zhuang, *The Institute of Statistical Mathematics*, Tokyo, *106*, 8569, (2006).
[14] A. Saichev, D. Sornette, Phys. Rev. Lett. **97**, 078501, (2006).
[15] A. Saichev, D. Sornette, J. Geophys. Res. **112**, B04313, (2007).
[16] D. Sornette, S. Utkin, A. Saichev, Phys. Rev. E **77**, 066109, (2008).
[17] M. Bottiglieri, L. de Arcangelis, C. Godano, E. Lippiello, Phys. Rev. Lett. **104**, 158501, (2010).
[18] S. Touati, M. Naylor, and I. G. Main, Phys. Rev. Lett. **102**, 168501, (2009).
[19] Y. Y. Kagan, Bull. Seism. Soc. Am. **94**, 1207–1228, (2004).
[20] M. Bottiglieri, E. Lippiello, C. Godano, and L. de Arcangelis, J. Geophys. Res. **116**, B02303, (2011).
[21] A. Helmstetter, Y.Y. Kagan and D.D. Jackson, J. Geophys. Res. **114** 110, B05S08, (2005).

[22] E. Lippiello, M. Bottiglieri, C. Godano, and L. de Arcangelis, Geophys. Res. Lett. **34**, L23301, (2007).
[23] E. Lippiello, C. Godano, and L. de Arcangelis, Phys. Rev. Lett. **98**, 098501, (2007).
[24] E. Lippiello, L. de Arcangelis, and C. Godano, Phys. Rev. Lett. **100**, 038501, (2008).
[25] E. Lippiello, L. de Arcangelis, and C. Godano, Phys. Rev. Lett. **103**, 038501, (2009).
[26] J. Davidsen and A. Green, Phys. Rev. Lett. **106**, 108502, (2011).
[27] E. Lippiello, C. Godano, and L. de Arcangelis, Geophys. Res. Lett. **39**, L05309, (2012).
[28] E. Hauksson, W. Yang, and P. Shearer: Waveform Relocated Earthquake Catalog for Southern California (1981 to 2011) `http://www.data.scec.org/research-tools/alt-2011-dd-hauksson-yang-shearer.html`
[29] W. H. Press, S. A. Teukolsky, W. T. Vetterling, and B. P. Flannery. Numerical Recipes in FORTRAN. Cambridge University Press, Cambridge, 2nd edition, 1992.
[30] A. Corral, Int. J. Mod. Phys. B **23**, 5570, (2009).
[31] J. M. Bland, and D. G. Altman, Brit. Med. J. **310**, 170, (1995).
[32] H. Abdi. In N.J. Salkind (Ed.): Encyclopedia of Measurement and Statistics. Sage, Thousand Oaks ,103–107, 2007.
[33] A. Corral, Phys. Rev. E **68**, 035102, (2003).
[34] K. R. Felzer and E. E. Brodsky, Nature **441**, 735–738, (2006).
[35] J. R. Holliday D. L. Turcotte, and J. B. Rundle, Pure Appl. Geophys. **165**, 1003, (2008).
[36] A. Helmstetter, *Phys. Rev. Lett.* **91**, 058501, (2003)

Eugenio Lippiello, Milena Bottiglieri, Cataldo Godano
Department of Environmental Sciences and CNISM
Second University of Naples
81100 Caserta, Italy

Àlvaro Corral
Centre de Recerca Matemàtica
Edifici Cc, Campus Bellaterra
E-08193 Bellaterra (Barcelona), Spain

Lucilla de Arcangelis
Department of Information Engineering and CNISM
Second University of Naples
81031 Aversa (CE), Italy

CRM Preprint Series number 1138

CRM
CENTRE DE RECERCA MATEMÀTICA
Facultat de Ciències, UAB
08193 Bellaterra
Barcelona, Spain
www.crm.cat